JLAB USER GROUP

Jefferson Lab PAC15
Proposal Cover Sheet

This document must be received by close of business Thursday,

Dec 17, 1998 at:

Jefferson Lab
User Liaison,
Mail Stop 12B
12000 Jefferson Ave.
Newport News, VA
23606

Experimental Hall: B

Days Requested for Approval: 30

Proposal Title:

Determination of the Sum of the Electric and Magnetic Polarizabilities of Pion using Polarized Photons

Proposal Physics Goals

Indicate any experiments that have physics goals similar to those in your proposal.

Approved, Conditionally Approved, and/or Deferred Experiment(s) or proposals:

Contact Person

Name: B. Norum
Institution: University of Virginia Physics Department
Address: 382 McCormick Road
Address:
City, State, ZIP/Country: Charlottesville, VA 22903 USA
Phone: 804-924-6789 **Fax:** 804-924-4576
E-Mail: ben@virginia.edu

Jefferson Lab Use Only

Receipt Date: 12/17/98 PR 99-010

By: [redacted]

BEAM REQUIREMENTS LIST

JLab Proposal No.: _____ Date: _____

Hall: _____ Anticipated Run Date: _____ PAC Approved Days: _____

Spokesperson: B. Norum, R. Hicks, K. Wang
Phone: 804-924-6789
E-mail: ben@virginia.edu

Hall Liaison: _____

List all combinations of anticipated targets and beam conditions required to execute the experiment. (This list will form the primary basis for the Radiation Safety Assesment Document (RSAD) calculations that must be performed for each experiment.)

Condition No.	Beam Energy (MeV)	Mean Beam Current (μA)	Polarization and Other Special Requirements (e.g., time structure)	Target Material (use multiple rows for complex targets — e.g., w/windows)	Material Thickness (mg/cm²)	Est. Beam-On Time for Cond. No. (hours)
1	6000	1.6		LH_2	1420	720

The beam energies, E_{Beam}, available are: $E_{Beam} = N \times E_{Linac}$ where N = 1, 2, 3, 4, or 5. E_{Linac} = 800 MeV, i.e., available E_{Beam} are 800, 1600, 2400, 3200, and 4000 MeV. Other energies should be arranged with the Hall Leader before listing.

LAB RESOURCES LIST

JLab Proposal No.: _____ Date _____
(For JLab OLO use only.)

List below significant resources — both equipment and human — that you are requesting from Jefferson Lab in support of mounting and executing the proposed experiment. Do not include items that will be routinely supplied to all running experiments such as the base equipment for the hall and technical support for routine operation, installation, and maintenance.

Major Installations *(either your equip. or new equip. requested from JLab)*

Compton High Intensity Photon Source (CHIPS)

New Support Structures: _____

Data Acquisition/Reduction

Computing Resources: _____

New Software: _____

Major Equipment

Magnets: _____

Power Supplies: _____

Targets: LH_2

Detectors: _____

Electronics: _____

Computer Hardware: _____

Other: _____

Other: _____

HAZARD IDENTIFICATION CHECKLIST

JLab Proposal No.: _____ Date: _____
(For CEBAF User Liaison Office use only)

Check all items for which there is an anticipated need.

Cryogenics ____ beamline magnets ____ analysis magnets _X_ target type: ____ flow rate: ____ capacity: ____	**Electrical Equipment** ____ cryo/electrical devices ____ capacitor banks ____ high voltage ____ exposed equipment	**Radioactive/Hazardous Materials** List any radioactive or hazadorous/ toxic materials planned for use: ____ ____ ____ ____
Pressure Vessels ____ inside diameter ____ operating pressure ____ window material ____ window thickness	**Flammable Gas or Liquids** type: ____ flow rate: ____ capacity: ____ **Drift Chambers** type: ____ flow rate: ____ capacity: ____	**Other Target Materials** ___ Beryllium (Be) ___ Lithium (Li) ___ Mercury (Hg) ___ Lead (Pb) ___ Tungsten (W) ___ Uranium (U) ___ Other (list below) ____ ____
Vacuum Vessels ____ inside diameter ____ operating pressure ____ window material ____ window thickness	**Radioactive Sources** ____ permanent installation ____ temporary use type: ____ strength: ____	**Large Mech. Structure/System** ____ lifting devices ____ motion controllers ____ scaffolding or ____ elevated platforms
Lasers type: NdYAG wattage: 10 W class: IV Installation: _X_ permanent ____ temporary Use: photon source ____ calibration ____ alignment	**Hazardous Materials** ___ cyanide plating materials ___ scintillation oil (from) ___ PCBs ___ methane ___ TMAE ___ TEA ___ photographic developers ___ other (list below) ____ ____	**General:** Experiment Class: ____ Base Equipment ____ Temp. Mod. to Base Equip. _X_ Permanent Mod. to Base Equipment _X_ Major New Apparatus Other: ____ ____

Determination of the Sum of the Electric and Magnetic Polarizabilities of the Pion using Polarized Photons

A. Cichocki, D. Higinbotham, R. A. Lindgren,
B. E. Norum, L. C. Smith, and K. Wang
University of Virginia, Charlottesville, Virginia

R. S. Hicks, D. Lawrence, R. A. Miskimen
G. A. Peterson and J. Shaw
University of Massachusetts, Amherst, MA

L.V. Fil'kov
Lebedev Physical Institute, Moscow,Russia

J. R. Calarco
University of New Hampshire, Durham, New Hampshire

H. Crannell, A. Longhi, J. T. O'Brien, and D. I. Sober
Catholic University of America, Washington, D.C.

L. Elouadrhiri
Christopher Newport University, Newport News, Virginia

R. Ent, and C. Keppel
Hampton University, Hampton, Virginia

J. Ficenec, and D.A. Jenkins
Virginia Poly Tech., Blacksburg, Virginia

I. Strakovsky
The George Washington University, Washington D.C.

T. P. Welch
Oregon State University, Corvallis, Oregon

M. Khandaker, V. Punjabi, and C. Salgado
Norfolk State University, Norfolk, Virginia

November 1998

Abstract

One month of beam time is requested in order to determine the sum of the electric and magnetic polarizabilities of the charged pion by measuring pion photoproduction, $\vec{\gamma}p \rightarrow \gamma\pi^+n$. The experiment will be performed using a liquid hydrogen target in the CLAS at Jefferson Laboratory, and will utilize linearly-polarized 600-1000 MeV photons produced by the Compton back-scattering from the electron beam of laser photons stored in a Fabry-Perot cavity. In addition to high linear polarization, the Compton source promises very high tagging efficiency and a low-background environment, features that, when combined with the comprehensive acceptance and excellent resolution of CLAS, permit the sum of the pion polarizabilities to be extracted with good precision. In particular, the large acceptance of CLAS provides the means to make essential checks on the reliability of the polarizability extraction.

1 Introduction

Electric (α) and magnetic (β) intrinsic polarizabilities characterize the induced transient dipole moments of hadrons subjected to external electromagnetic fields. They are a measure of the rigidity of the internal structure of baryons and mesons, as directly probed, for example, in $\gamma-$hadron Compton scattering. As such, polarizabilities are fundamental quantities predicted by models of hadrons. Due to its light mass and the relative simplicity of the $q\bar{q}$ system, the polarizabilities of the pion are especially important. Indeed, calculations for the pion have been performed using a variety of models, such as the work of Bernard, Hiller, and Weise[1] emphasizing vector meson dominance diagrams, and Bernard et al. [2] within generalized SU(3) models. Another theoretical approach is based on the s-channel ($\gamma\pi \rightarrow \gamma\pi$) and t-channel ($\gamma\gamma \rightarrow \pi\pi$) dispersion sum rules[3] [4]. For the $\gamma - \pi$ interaction at low energy, Chiral Perturbation Theory (ChPT) provides a rigorous way to make predictions, because it is obtained directly from QCD and relies only on the solid assumptions of spontaneously broken $SU(3)_L \times SU(3)_R$ chiral symmetry, Lorentz invariance, and low momentum transfer [5].

Experimental determinations of the pion polarizabilities are especially challenging since no stable target is available, and indirect processes are required. Moreover, background contributions are always present. For charged pions, three experimental methods have been used: radiative pion-nucleon scattering $\pi N \rightarrow \pi N\gamma$, pion photoproduction in photon-nucleon scattering $\gamma N \rightarrow \gamma N\pi$, and $\gamma\gamma \rightarrow \pi\pi$ as observed in e^+-e^- colliding interactions. Nevertheless, due to background uncertainties and model dependence in the analysis procedures, existing results lack consistency and are generally imprecise.

Chiral symmetry is a property of QCD manifested in the low energy interactions of hadrons. In this domain it has enjoyed much success, and, most particularly for the lightest hadron, the pion, is expected to give reliable predictions for the polarizabilities. Indeed, any disagreement would raise serious questions about our understanding of low-energy QCD [6]. In the chiral symmetry limit of zero quark mass, ChPT predicts the electric and magnetic

polarizabilities of the charged pion to be

$$\bar{\alpha}_E^{\pi^\pm} = -\bar{\beta}_M^{\pi^\pm} = (2.8 \times 10^{-4} \pm 0.5)\mathrm{fm}^3.$$

Most experimental determinations have failed to confirm this prediction. In view of the close connection between ChPT prediction and the underlying validity of QCD, any discrepancy would be considered serious. As emphasized by Holstein [7] that "*indeed if QCD is the correct model for the interactions of quarks and gluons then the low energy predictions described here which are predicted on chiral symmetry must obtain. Correspondingly if a strong violation of one or more of these predictions is confirmed, it will be very difficult to reconcile with QCD. Thus the stakes are high and this makes such tests all the more interesting and important*".

We are proposing an experimental test of the π^+ polarizabilities by measuring $\gamma p \to \pi^+ n\gamma$ scattering with photons derived from the Compton backscattering source proposed for Hall B, a facility which promises to provide tagged photons with energies up to 1.1 GeV (for a 6 GeV electron beam) and linear polarizations in excess of 90%. The experiment will be most sensitive to the polarizability sum $\bar{\alpha} + \bar{\beta}$. As with the ChPT predictions noted above, all existing theoretical treatments indicate that this sum should be close to zero, however these predictions have never been adequately tested. The proposed investigation will complement experiments planned at CERN, Frascati, and at Mainz.

2 Theoretical Models

Polarizability is a classical concept which describes the extent to which a system is polarized in the presence of an external electromagnetic field. When an external electric field $\vec{E}$ induces an electric dipole moment

$$\vec{p} = 4\pi\alpha\vec{E} \ ,$$

the constant α is identified as the electric polarizability. Similarly, the magnetic polarizability β is defined by

$$\vec{\mu} = 4\pi\beta\vec{H}.$$

In an atomic system, for example, the electric and magnetic polarizabilities are directly related to the index of refraction, which describes forward photon scattering. Therefore, the polarizabilities can be investigated by means of Compton scattering. Traditionally, the polarizabilities have been split into an intrinsic contribution, α or β, given by the sum over all possible dipole transitions to excited states, and an additional term, $\Delta\alpha$ or $\Delta\beta$, representing recoil, retardation, and relativistic effects[5], *e.g.*

$$\bar{\alpha} = \alpha + \Delta\alpha \ .$$

In non-relativistic theory, the latter term is determined by the electric rms radius of the pion,

$$\Delta\alpha = (\alpha_e/3\mu) < r_\pi^2 > \approx 15 \times 10^{-4} \text{ fm}^3,$$

where α_e is the fine structure constant and μ the pion mass. The recoil term $\Delta\alpha$ is positive and if, according to some models, it is larger than values predicted for $\bar{\alpha}$, the intrinsic electric polarizability should be negative[6]. This is speculated to arise from negative-energy intermediate states involving quark sea components[8] in the pion wave function and from disconnected diagrams for the dissociation of a photon into a particle-antiparticle pair. Holstein[6] has associated a sizable negative intrinsic polarizability with vector meson contributions, noting that meson exchange via an axial meson pole diagram provides the essential contribution to the polarizability. Various theories predict rather different values for the pion polarizabilities. For example, an early

evaluation of the polarizability difference $\bar{\alpha} - \bar{\beta}$ by application of the dispersion sum rule (DSR) at finite energy[3] gave $(\bar{\alpha} - \bar{\beta})_{\pi^\pm} = 10.6 \times 10^{-4}$ fm^3. This is consistent with the DSR result of $(\bar{\alpha} - \bar{\beta})_{\pi^\pm} = 10.9 \times 10^{-4}$ fm^3 obtained at a fixed value of the Mandelstam variable $u = \mu^2$[3], but disagrees strongly with the result of a calculation in the linear σ-model with quarks and vector mesons which gave[1]

$$(\bar{\alpha} - \bar{\beta})_{\pi^\pm} \approx 20 \times 10^{-4} \text{ fm}^3.$$

An even larger value was obtained in the Nambu-Jona-Lasinio model[2], leading to the conclusion that the polarizability should be essentially described by the classical finite size term, $\bar{\alpha}_{\pi^\pm} \approx \Delta\alpha$. ChPT has been particularly successful in describing low energy hadronic properties, and provides a firm prediction of the pion polarizabilities. If this prediction were shown to be in error, grave concerns would be raised regarding the validity of low-energy QCD[7]. Because it is obtained directly from QCD and relies only on the fundamental assumptions of spontaneously broken $SU(3)_L \times SU(3)_R$ chiral symmetry, ChPT provides rigorous predictions for the $\gamma - \pi$ interaction at low energy. Unitarity is achieved by adding low-order pion loop corrections, and the resulting infinite divergences are absorbed into physical (renormalized) coupling constants[9, 10]. By means of a perturbative expansion of momenta and quark masses, the method establishes relationships between different processes. For example, at order $\mathcal{O}(p^4)$ the charged pion polarizabilities are simply related to radiative pion beta decay $\pi^+ \to e^+\nu_e\gamma$ by[10]

$$\frac{\alpha_e h_A}{\sqrt{2}F_\pi \mu} = \bar{\alpha} = -\bar{\beta} = (2.8 \pm 0.5) \times 10^{-4} \text{ fm}^3 \ , \tag{1}$$

where $F_\pi = 93.1$ MeV[11] is the pion decay constant, $h_A = (0.0117 \pm 0.0020)\mu^{-1}$ is the axial vector coupling constant, and α_e is the fine structure constant. In the ChPT predictions, contributions of negative sign to the intrinsic polarizability cancel positive contributions from vector mesons to the finite size terms,[12, 13] leaving only the relatively small component belonging to axial mesons[6]. Beginning at order $\mathcal{O}(p^6)$, additional terms appear in Eq. 1. For example, at order $\mathcal{O}(p^6)$, ChPT predicts that a polarizability sum of

$$(\bar{\alpha} + \bar{\beta})_{\pi^\pm} = 0.3 \times 10^{-4} \text{fm}^3 \ ,$$

compared to the null result obtained at $\mathcal{O}(p^4)$. It remains to be shown whether the cumulative effect of $\mathcal{O}(p^6)$ and higher-order corrections modify the $\mathcal{O}(p^4)$ predictions significantly. The convergence properties of ChPT are tested more conclusively with the pion. Dispersion sum rules have also been utilized to predict pion polarizabilities. For charged pions, for example, $s-$channel ($\gamma\pi \to \gamma\pi$) and t-channel ($\gamma\gamma \to \pi\pi$) analyses[3, 4] give

$$\bar{\alpha} + \bar{\beta} = (0.39 \pm 0.04) \times 10^{-4}\ \mathrm{fm}^3,$$

and

$$\bar{\alpha} - \bar{\beta} = 10.8 \times 10^{-4}\ \mathrm{fm}^3,$$

implying $\bar{\alpha} = 5.6$ and $\bar{\beta} = -5.2$. Because of the difficulties in evaluating the high-energy asymptotic contributions, these results are model-dependent. Pion polarizabilities have also been evaluated in the Dubna quark confinement model[14], with the result $\bar{\alpha} = 3.63$. These and other predictions are listed in Table 1. Whereas varying values are obtained for the individual electric and magnetic polarizabilities, the different theories concur that the sum of the polarizabilities $\bar{\alpha}_\pi + \bar{\beta}_\pi$ of the charged pion should be small. The reason for this is that the lowest order contributions of the internal structure to an effective Lagrangian depend on the electromagnetic fields E and B according to $\mathcal{L}_{eff} \sim F_{\mu\nu}F^{\mu\nu} \sim E^2 - B^2$, hence $\bar{\alpha} = -\bar{\beta}$ [7]. All higher order contributions involve additional gradients in the Lagrangian, *i.e.* momenta and mass terms, which are small near threshold due to the small mass of the pion.

3 Experimental Results

In the absence of a free pion or photon target, experimental studies of pion polarizability must be made indirectly, relying on virtual target particles. For example, with an incident beam of real photons, the elementary Compton scattering process shown as Fig. 1*a* can be accessed as one of the two vertices of the diagram represented in Fig. 1*b*, where the target is a virtual pion in the pion field of a proton. At small values of $|t|$, the squared invariant mass of the virtual pion, the interaction takes place at a relatively large distance from the proton, and is mediated by a single pion. The reaction represented by Fig. 1*b* can be measured over a wide kinematic range, and, in principle, all three final products can be detected. Although this aids the separation of the two vertices, the desired cross section lies at the pion pole in an experimentally inaccessible region, and recourse is needed to a model-dependent extrapolation procedure, such as the Chew-Low[15] method.

In an alternative method of radiative pion scattering, an incident high-energy pion scatters from a virtual photon in the electromagnetic field of a nucleus, as represented in shown in Fig. 1*c*. In this case[16] extrapolation is also required, however, in an entirely physical parameter, the four-momentum squared: $Q^2 \to 0$. The primary disadvantage of this technique is the large hadronic backgrounds: Compton scattering is electromagnetic, whereas the interaction of the pion with the target is predominantly by means of the strong force.

Compton scattering from the pion also occurs in high-energy e^+-e^- collisions, by means of the reaction $\gamma\gamma \to \pi^+\pi^-$ represented in Fig. 1*d*. The Compton amplitude in this case is obtained by crossing symmetry. At threshold the reaction depends heavily on the s-wave $\pi - \pi$ interaction, and the threshold cross section is modeled by fitting data in the kinematic region $S_1 < -\mu^2$ and $t_1 > 4\mu^2$, where s_1 and t_1 are the square of the total energy, and the momentum transfer in the $\gamma\pi$-channel, respectively. The result of this fit is then extrapolated to the point $S_1 = \mu^2$, $t_1 = 0$ of the reaction $\gamma\pi \to \gamma\pi$ in order to determine the pion polarizabilities. The extrapolation is over a large range and model-dependent[17].

All three methods outlined above have been exploited in order to obtain information on the pion polarizabilities. For example, pion photoproduction was measured[18] at the Lebedev Institute with bremsstrahlung photons ranging from 350 to 800 MeV. All three final products, γ, π^+, and n were detected using small solid-angle detectors. There was no tracking of charged particles and statistics were limited to 2200 events extracted from 147k raw data events. The deduced electric polarizability, obtained under the assumption $\bar{\alpha} + \bar{\beta} = 0$, was $\bar{\alpha} = (20 \pm 12) \times 10^{-4}\text{fm}^3$.

Radiative pion scattering was measured[19, 20] at Serpukov with a 40 GeV π^- beam on targets of Be, C, Al, Fe, Cu, and Pb. From 2100k raw data events, 7k Compton events were identified over a wide range of photon scattering angles. For photons backward-scattered in the pion rest frame, the polarizability contribution to the Compton cross section is proportional to $\bar{\alpha} - \bar{\beta}$. For forward scattered photons, polarizability contributes as $\bar{\alpha} + \bar{\beta}$. By analyzing data over the extended angular range, Antipov *et al.*[19, 20] obtained

$$\bar{\alpha} - \bar{\beta} = (13.6 \pm 2.8) \times 10^{-4}\text{fm}^3,$$

and

$$\bar{\alpha} + \bar{\beta} = (1.4 \pm 3.1 \pm 2.5) \times 10^{-4}\text{fm}^3 \ .$$

Two-photon interactions observed in $e^- - e^+$ collisions have been measured at several facilities, including PLUTO, DM1, DM2, MARK2[21, 22, 23, 24, 25]. Unfortunately, statistics are typically poor and a discrepant range of answers has resulted. Nevertheless, impressive precision has been reported in some of these analyses. For example, assuming $\bar{\alpha}+\bar{\beta} = 0$, Babusci *et al.*[5] extracted a charged pion polarizability of $\bar{\alpha} = (2.2 \pm 1.6) \times 10^{-4}$ fm^3 from data obtained with the MARK2 detector. However, the precision claimed in this result seems unduly optimistic in light of a subsequent theoretical study[10]. Even more striking results have been obtained by analyses of $\gamma\gamma \to \pi\pi$ data that employ dispersion sum rules. For example, from the same MARK2 data, Kaloshin *et al.*[26] derived a value of $\bar{\alpha} + \bar{\beta} = (0.22 \pm 0.06) \times 10^{-4}$ fm^3 for the charged-pion polarizability sum. Such analyses are acknowledged to have considerable model sensitivity, and have received severe criticism. For example, in the DaΦne handbook Portoles and Pennington[27] conclude that *the only way to measure the pion polarizabilities is in the Compton scattering process near threshold and not in* $\gamma\gamma \to \pi\pi$.

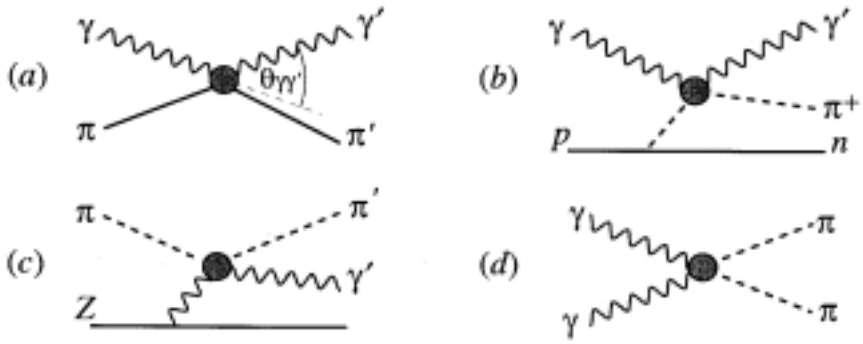

Figure 1: Diagrams for pion Compton scattering. (a) Elementary diagram; (b) radiative pion photoproduction; (c) radiative pion scattering; and (d) diagram for double pion production in two photon scattering.

As revealed by the summary presented in Table 1, notwithstanding significant effort, the present experimental information on the polarizabilities of the pion is unsatisfactory. More accurate and reliable determinations are needed to test the precise predictions provided by recent theoretical advances, such as ChPT. Accordingly, a new round of experimental studies have been proposed including radiative pion scattering at COMPASS (CERN) and pion photoproduction using tagged photons at Mainz[28]. A pion photoproduction using tagged polarized photons with CLAS can complement these studies. In particular, the similar experiment at Mainz is configured for backward-scattered photons and will therefore be primarily sensitive to the polarizability difference. On the other hand, with CLAS there is large acceptance to forward-scattered photons, allowing us to greatly improve experimental information on the polarizability sum. The nearly 4π CLAS detector is of considerable benefit in this regard, and the availability of a highly polarized photon beam will enhance the polarizability contribution while, at the same time, diminishing backgrounds.

The polarizabilities of the pion have heretofore resisted precise determination and none of the experiments listed above will be easy. As previously noted, irrespective of the experimental method, large backgrounds are always present. Moreover, even when the Compton amplitude is isolated, the contribution of the polarizabilities constitutes only a small correction to the dominant Born term. Nevertheless, by means of a multi-pronged attack that draws upon the diverse strengths of different facilities, we can expect that the experimental situation regarding the pion polarizabilities will be significantly improved during the next few years. CLAS offers the opportunity to make a notable contribution to this progress.

Model	Data	Reaction	$\bar{\alpha}$ $(10^{-4} fm^3)$	Ref.
ChPT			2.7	[7]
DSR			5.6	[3]
Bernard			7-14	[1][2]
	Lebedev	$\gamma p \to \gamma \pi^+ n$	20 ± 12	[18]
	Serpukov	$\pi^- A \to \gamma \pi^- A$	$6.8 \pm 1.4 \pm 1.2$	[19]
	PLUTO	$\gamma\gamma \to \pi^+\pi^-$	$19.1 \pm 4.8 \pm 5.7$	[21]
	DM1	$\gamma\gamma \to \pi^+\pi^-$	17.2 ± 4.6	[22]
	DM2	$\gamma\gamma \to \pi^+\pi^-$	26.3 ± 7.4	[23]
	MARK II	$\gamma\gamma \to \pi^+\pi^-$	2.2 ± 1.6	[24]
	Data	Reaction	$\bar{\alpha} + \bar{\beta}$	Ref.
	Serpukov	$\pi^- A \to \gamma \pi^- A$	$1.4 \pm 3.1 \pm 2.8$	[19]
	Data	Reaction	$\bar{\alpha} - \bar{\beta}$	Ref.
	Serpukov	$\pi^- A \to \gamma \pi^- A$	13.6 ± 2.8	[19]

Table 1: Values of $\bar{\alpha}$ for $\pi^\pm$ from data and model.

4 Kinematics and Cross Sections

4.1 Kinematics

The reaction from which we seek to determine the pion polarizabilities is $\vec{\gamma}p \rightarrow \gamma\pi^+n$. As defined in Fig. 1*b*, the 4-momentum of the incoming photon in the laboratory system is $k_1 = (\vec{k}, k)$, and $k_2 = (\vec{k}', k')$ for the outgoing photon. Other four-momenta are $q = (\vec{q}, E)$ for the pion, $P_1 = (0, M_p)$ for the target proton, and $P_2 = (\vec{P}_2, E_2)$ for the recoil neutron. We set M_p, M_n, and μ to represent the masses of the proton, neutron, and pion. For incident tagged photons, we can reconstruct all kinematics if we know the 4-momenta of any two reaction products. Two other reconstructed variables serve to describe the multi-particle system. The first is the 4-momentum transfer delivered to the neutron. This is equal to the squared invariant mass of the off-shell pion, and is represented by

$$t = (M_n - M_p)^2 - 2T_n M_p, \tag{2}$$

where T_n is the kinetic energy of the neutron. Neglecting the p-n mass difference, t is negative and proportional to T_n. For an on-shell pion, $t = \mu^2$, the location of the pion pole. The variable t specifies the off-shell mass of the struck virtual pion, and it is the variable over which extrapolation is made to obtain the Compton scattering cross section for a free pion. By restricting data to small t, we ensure that the measured reaction is mediated by one-pion exchange. The other variable of importance is S_1, the squared invariant mass of the $\gamma - \pi^+$ system:

$$S_1 = (k' + E)^2 - (\vec{k}' + \vec{q})^2 \ . \tag{3}$$

The lower limit of S_1 is $1\mu^2$, and the higher limit is set by the incoming photon energy. It is convenient to use μ^2 as the unit of t and S_1. From the phase-space of t and S_1, shown in Fig. 2, we see that at constant S_1 higher photon energies give access to the smaller $|t|$-values that are favorable for making reliable extrapolations. Three other independent kinematic variables are S, the squared invariant mass of the initial state, t_1, the 4-momentum transfer delivered to the pion, and S_2, the squared invariant mass of the the

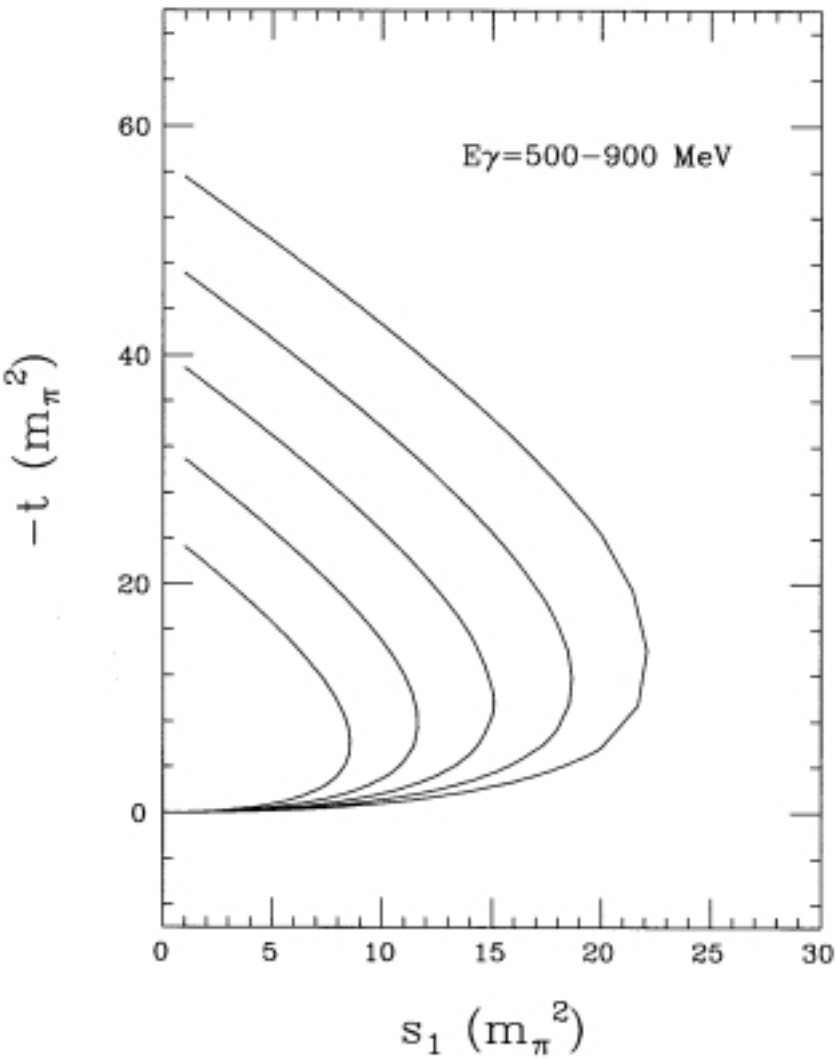

Figure 2: For t-channel pion photoproduction the allowed phase space lies within the contours. The smallest (inner) contour belongs to 500 MeV photons and the largest to 900 MeV. Contours are indicated for 100 MeV energy increments.

pion-neutron system:

$$\begin{aligned} S &= (k_1 + P_1)^2 \ , \\ t_1 &= (k_2 - k_1)^2 \ , \\ S_2 &= (q + P_2)^2. \end{aligned} \tag{4}$$

4.2 Scattering of Unpolarized Photons from Free Pions

The differential cross section for the Compton scattering of an unpolarized photon from a free charged pion can be written[17]:

$$\begin{aligned} \frac{d\sigma_{\gamma\pi}}{d\Omega} &= \left(\frac{d\sigma_{\gamma\pi}}{d\Omega}\right)_B - \frac{e^2(S1-1)^2}{16\pi \cdot S_1^2[(S_1+1)+(S_1-1)z]} \cdot \\ & [(1-z)^2(\bar{\alpha}-\bar{\beta}) + S_1^2(1+z)^2(\bar{\alpha}+\bar{\beta})] + ... \end{aligned} \tag{5}$$

where $z = \cos\theta_{\gamma\gamma}^{cm}$. The leading-order Born term gives the threshold cross section. This Thomson limit is defined by the charge of the pion. The polarizabilities enter as corrections, beginning with the next term that represents the interference with the Born amplitude. Equation 5 shows that backward scattering, *i.e.* negative z, favors the polarizability difference $\bar{\alpha}-\bar{\beta}$, while forward scattering, *i.e.* positive z, favors the polarizability sum $\bar{\alpha}+\bar{\beta}$. Although the polarizability sum is expected to be small relative to the difference, its contribution is enhanced for S_1 even slightly removed from threshold. The Born cross section depends only on S_1 and the center-of-mass photon scattering angle. For unpolarized photons it is[29]

$$\left(\frac{d\sigma_{\gamma\pi}}{d\Omega}\right)_B = \left(\frac{e^4}{4\pi}\right)^2 \frac{1}{S_1} \frac{(S_1^2+1)(1+z^2)+2(S_1^2-1)z}{[S_1+1+(S_1-1)z]^2}. \tag{6}$$

4.3 Scattering of Linearly-Polarized Photons from Free Pions

When the plane of polarization of an incident linearly-polarized photon beam is in the scattering plane, the Compton cross section is[17]

$$\begin{aligned}\frac{d\sigma_{\parallel}}{d\Omega} &= \left(\frac{e^2}{4\pi}\right)^2 \frac{1}{S_1}\left(1-\frac{2S_1(1+z)}{(S_1+1)+(S_1-1)z}\right)^2 - \frac{e^2}{4\pi}\frac{(S_1-1)^2}{4S_1^2}\times \\ &\left(1-\frac{2S_1(1+z)}{(S_1+1)+(S_1-1)z}\right)\times \\ &\left[(1-z)(\bar{\alpha}-\bar{\beta})-S_1(1+z)(\bar{\alpha}+\bar{\beta})\right]+\ldots \qquad (7)\end{aligned}$$

For photons polarized perpendicular to the scattering plane the cross section is

$$\frac{d\sigma_{\perp}}{d\Omega} = \left(\frac{e^2}{4\pi}\right)^2 \frac{1}{S_1} - \frac{e^2}{4\pi}\frac{(S_1-1)^2}{4S_1^2}\left[(1-z)(\bar{\alpha}-\bar{\beta})+S_1(1+z)(\bar{\alpha}+\bar{\beta})\right]+\ldots \quad (8)$$

As in the case of unpolarized incident photons, the cross section is seen to be sensitive to $\bar{\alpha}-\bar{\beta}$ for backward scattering and to $\bar{\alpha}+\bar{\beta}$ for forward scattering at large S_1. Inspection of these equations further reveals that for a scattering angle given by

$$z = z_0 = -\frac{S_1-1}{S_1+1}, \qquad (9)$$

the interference contribution to the cross section for parallel polarization vanishes. For $5 < S_1 < 10$ the corresponding center-of-mass scattering angle varies from 132° to 145°. Measurements at this backward scattering angle could be utilized to check the reliability of the extrapolation procedure and the known Born cross section should be obtained. In principle, higher-order terms such as $\bar{\alpha}^2$ would modify this expectation, but the effect would be difficult to observe. At this same angle z_0, only the electric polarizability $\bar{\alpha}$ contributes to the cross sections for unpolarized photons and for perpendicularly-polarized photons. In principle then, by means of precision measurements at z_0, the electric polarizability of the pion could be uniquely determined. More generally however, the availability of precision

data over an extended range of photon scattering angles $\theta_{\gamma\gamma}^{\rm cm}$ would permit both polarizations, $\bar{\alpha}$ and $\bar{\beta}$, to be determined. This holds *independent* of the polarization properties of the incident photon. Figure 3 shows the angular dependence of the Compton scattering differential cross section for two values of S_1 and various values of $\bar{\alpha}-\bar{\beta}$ and $\bar{\alpha}+\bar{\beta}$; The Born term is represented by $\bar{\alpha}-\bar{\beta}=\bar{\alpha}+\bar{\beta}=0$. Three conclusions may be drawn from these graphs: The polarizability contribution to the cross section increases with increasing S_1; the sensitivity to $\bar{\alpha}+\bar{\beta}$ at forward angles is considerably greater than the sensitivity to $\bar{\alpha}-\bar{\beta}$ at backward angles; and perpendicularly-polarized incident photons are most sensitive to pion polarizability.

A favorable condition to determine $\bar{\alpha}+\bar{\beta}$ hence occurs for perpendicularly polarized photons scattering at relatively forward angles with values of S_1 not too close to threshold. A further advantage of perpendicular polarization, indicated by calculations of Drechsel and Fil'kov[17], is that the contribution of diagrams that constitute a background to the t-channel diagram are decreased. Such an experiment is well-suited to CLAS, especially with the availability of highly-polarized photons from the Compton back-scattering source. Moreover, the comprehensive angular acceptance of CLAS provides simultaneous detection of all possible alignments of the photon polarization angle with respect to the scattering plane. The enhanced sensitivity to $\bar{\alpha}+\bar{\beta}$, indicated by Fig. 3, provides a severe test of theoretical notions that $\bar{\alpha}+\bar{\beta}\approx 0$. As we will see, another, more practical, reason for not setting as our primary objective the determination of the polarizability difference $\bar{\alpha}-\bar{\beta}$ is that at very backward scattering angles, where this combination is emphasized, the pion recoils close to the beam-pipe in the forward direction, where it escapes detection.

4.4 Pion Photoproduction

As previously noted, the free $\gamma-\pi$ scattering cross section is not measured directly, but instead through the reaction $\gamma p\to\gamma\pi^+ n$. In the late fifties Chew and Low[15] showed how unstable particles, *e.g.* virtual pions in the pion cloud of a nucleon, could serve as targets for scattering experiments. When $|t|$, the squared invariant mass of the virtual pion, is small, it is relatively

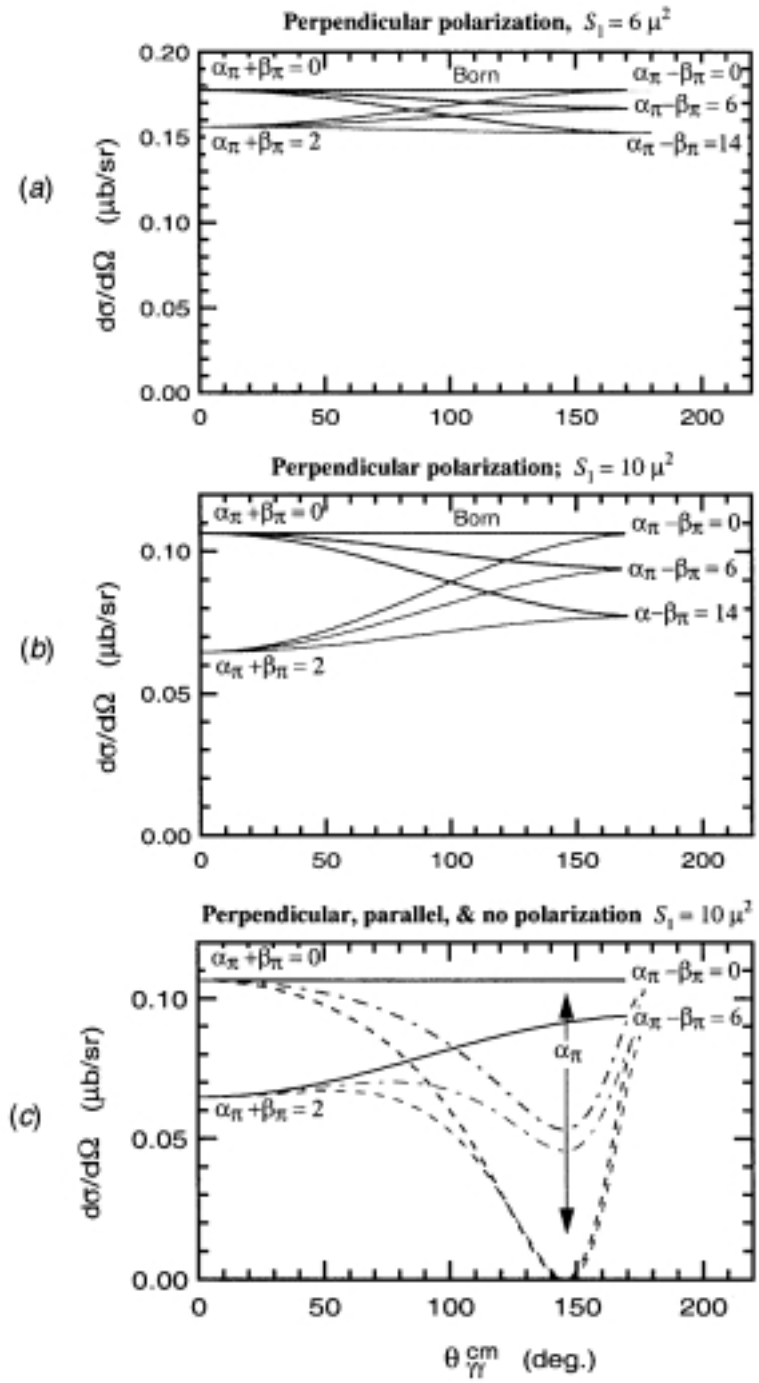

Figure 3: Cross sections for π^+ Compton scattering for different polarization state and S_1.

distant away from the nucleon, and in interacting with an external particle may gain sufficient energy to escape as a real pion. In order to obtain the free pion cross section an extrapolation in t is needed to the pion pole at $t = +\mu^2$, whereas the physical region accessed in such an experiment is restricted to $t < 0$. This technique has been successfully employed to determine the pion-nucleon coupling constant through $\gamma p \to \pi^+ p$ reaction[30], as well as from N-N scattering[31]. It is also used in the determination of $\pi\pi \to \pi\pi$ scattering from the $\pi p \to \pi\pi p$ reaction[32]. The method will be also used in JLab experiments 94-105, a chiral anomaly study[33].

In the present case, the Chew-Low relation between the γp and $\gamma\pi$ cross sections may be expressed as[34]:

$$\lim_{t\to 1} \frac{d^2\sigma_{\gamma p\to\gamma\pi N}}{dt ds_1 d\Omega} = \frac{g^2}{4\pi}\frac{(s_1-1)}{8\pi M_p^2 E_\gamma^2}\frac{(-t)}{(t-1)^2}G_A^2(t)\left(\frac{d\sigma}{d\Omega}\right)_{\gamma\pi\to\gamma\pi} \tag{10}$$

where $g^2/4\pi = 14.7$ is the pion-nucleon coupling constant and the axial form factor of the nucleon $G_A^2(t)$ is normalized to unity at $t = 0$. The γp cross section depends on the $N\pi N$ and $\gamma\pi$ vertices and a t-channel propagator. For the purpose of illustration, we assume that the above relation holds for values of t moved away from the pion pole. The corresponding t-channel cross section is plotted in Fig. 4 as a function of t for $E_\gamma = 700$ MeV and $S_1 = 6$. The cross section passes through zero at $t = 0$, rises to a maximum at $t = -1$, and then decreases. The t-channel cross section is seen to be large near $t = -1$, and very small for $t \approx 0$. Multiplying the γp cross section by the pole term $(t-1)^2$, we define

$$F(t) \;=\; \frac{d^2\sigma_{\gamma p\to\gamma\pi N}}{dt dS_1 d\Omega}\times(t-1)^2 \Rightarrow -\frac{g^2}{4\pi}\frac{(S_1-1)^2}{8_p^2 E_\gamma^2}tG_A^2(t)\left(\frac{d\sigma}{d\Omega}\right)_{\gamma\pi\to\gamma\pi} \tag{11}$$

a straight line passing through the origin. This proportional t-dependence results from the the nature of pseudoscalar one-pion exchange. For a pure t-channel process then, the extrapolation to the pion pole at $t = 1$ simply follows a straight line. At the pole,

$$F(t=1) = -\frac{g^2}{4\pi}\frac{(S_1-1)}{8\pi M_p^2 E_\gamma^2}G_A^2(t)\left(\frac{d\sigma}{d\Omega}\right)_{\gamma\pi\to\gamma\pi}, \tag{12}$$

and

$$\frac{d\sigma_{\gamma\pi}}{d\Omega} = -K(S_1, E_\gamma) \times \lim_{t\to 1} F(t) \ , \tag{13}$$

where

$$K(S_1, E_\gamma) = \frac{32\pi^2 E_\gamma^2 M_p^2}{g^2(S_1 - 1)} \ . \tag{14}$$

In practice, as the pion moves off the mass shell the two vertices become described by form factors and accordingly $F(t)$ becomes more complicated. Moreover, at larger values of $|t|$ reaction diagrams other than the t- channel process contribute, such as s-channel, u-channel, and two-pion exchange. Calculations of these processes are model-dependent.

4.5 Extraction of Pion Polarizability

Reliable extrapolation demands the availability of statistically precise data extending to values of $-t$ that are as close to zero as possible. As indicated in Fig. 2, the lower limit of $-t$ accessible in this experiment is set by the photon energy and S_1. The t-channel cross section has been shown to reach a maximum at $t = -1$, for which the kinetic energy of the recoil neutron is approximately 10 MeV. Much smaller values of $-t$ are difficult to access because the neutron kinetic energy diminishes and the range of the time-of-flight TDCs precludes the detection. Small values of $-t$ are best measured at higher photon energies; however, count rates decrease since the cross section is proportional to $1/{E_\gamma}^2$. Also demanding care is the presence of singularities in the extrapolation path. Drechsel and Fil'kov[17] have described how the effect of such singularities can be minimized by constructing subsets of the data having fixed values of the kinematic parameters E_γ, S_1, t_1 and S_2. The comprehensive acceptance of CLAS makes this requirement easy to meet. Figure 5 shows an example of quality of data expected in this experiment, as well as the results of two linear extrapolation fits.

Much effort has been invested to test the reliability of the extrapolation procedure. Here we will briefly summarize the findings. Pseudodata, generated

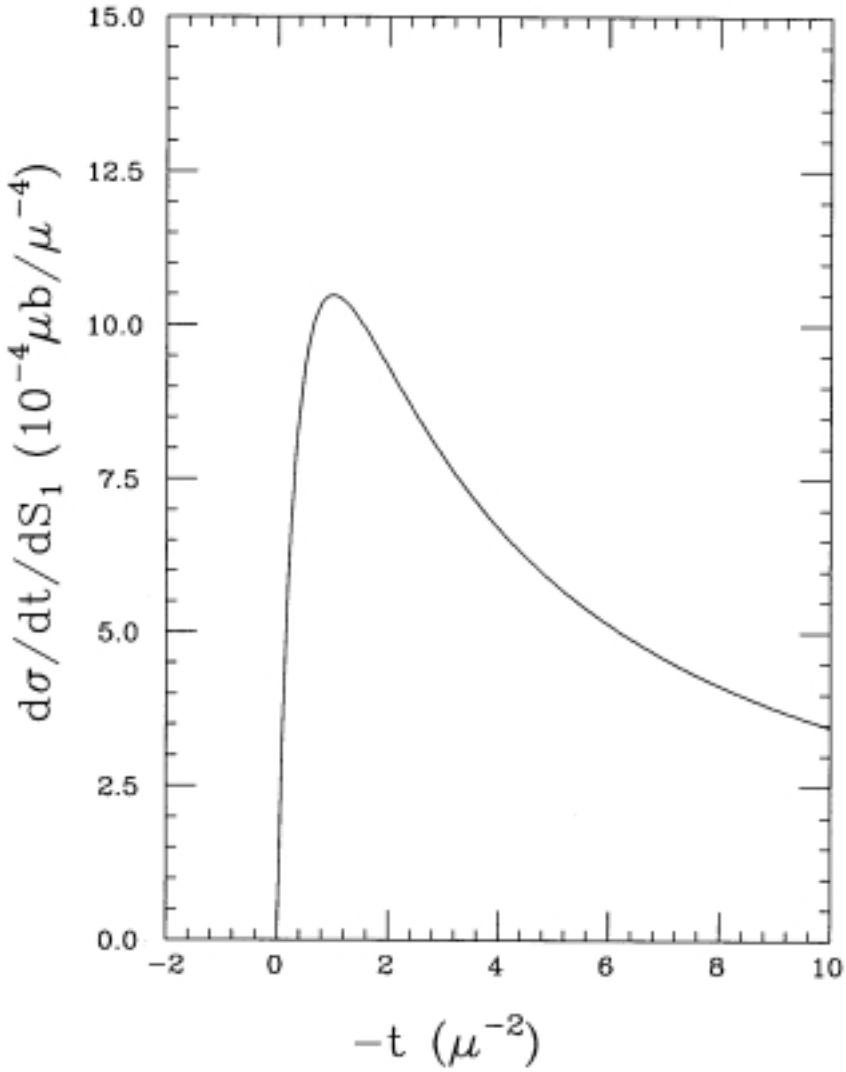

Figure 4: t-dependence of the total cross section in the $\gamma p \to \gamma \pi^+ n$ reaction with pure OPE for $E_\gamma = 0.7$ GeV and $S_1 = 6$.

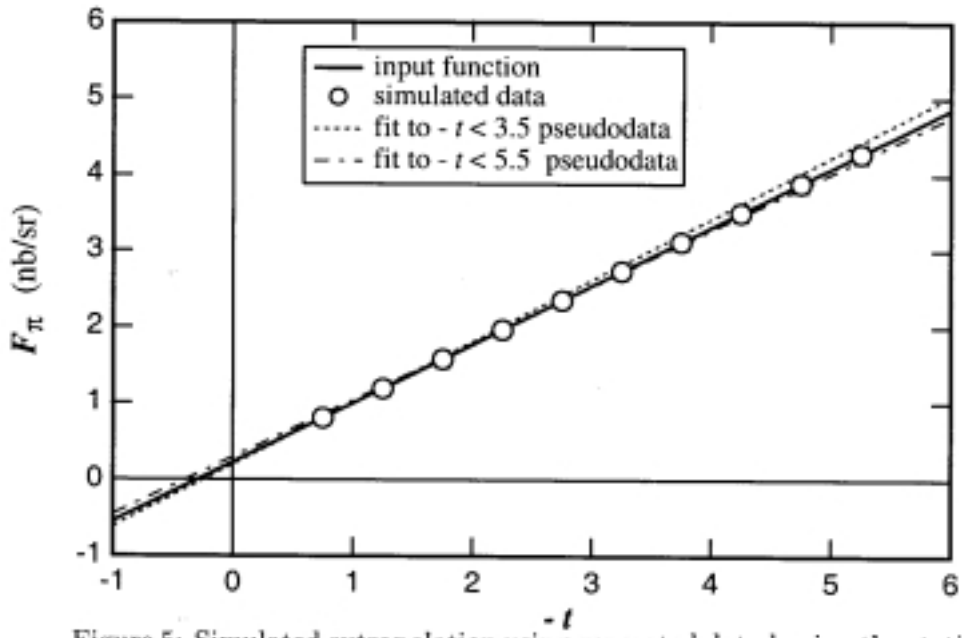

Figure 5: Simulated extrapolation using generated data having the statistical accuracy projected for the kinematic range $7 < S_1 < 8$. The solid curve is the assumed input function, the dashed and dash-dotted curves show fits and extrapolations for two limits of t. Both S_1 and t are in units of the pion mass squared.

in the physical $-t$ region using a variety of models, have been extrapolated to the pion pole using polynomial expansions and Pade approximant of various orders. The extrapolation error is determined from the error matrix for the extrapolation fit. These simulations show that the extrapolation is reliable *provided it is made over a region in t for which the function $F(t)$ remains close to linear.*

When curvature in $F(t)$ dictates fitting with a quadratic polynomial or Pade approximant, the extrapolation becomes unreliable: not only does the extrapolation uncertainty increase markedly, but the pole cross section of the generating function is not reproduced within this magnified error. Just how linear is the function $F(t)$ in the region of extrapolation? As has been shown, if only the t-channel diagram were present, $F(t)$ would be perfectly linear. Because only published data[18] in this region are uninstructive due to very large statistical errors, one turns to the theoretical evaluations of Fil'kov[28], which include many of the important background diagrams. An example of these calculations, shown in Fig. 6 indicates that $F(t)$ remains close to linear up to $-t = 3.5$. More detailed calculations recently made suggest that the linearity persists up to at least $-t = 5$. We have found that a 10% quadratic change over the fitting range introduces an uncertainty in the extracted polarizability parameter that is comparable to the overall statistical uncertainty. However, to date calculations have been made only for backward photon scattering, not for the forward-scattering that is the emphasis of this proposal. In any case, whatever the kinematics, the t-dependence of $F(t)$ can only be confirmed by experiment.

An alternative way to investigate the pion polarizability is suggested by Fig. 6. This shows the polarizability contribution to the cross section in the physical region for $S_1 = 6$. At larger S_1 the polarizability contribution is enhanced; at small S_1 the polarizability contribution becomes negligible. In the CLAS experiment we propose, data will be simultaneously acquired throughout this comprehensive range in S_1. The low-S_1 results can be used to test and refine the best available theoretical evaluations of threshold pion photoproduction. Observed departures from these predictions at large S_1 could be used to assess any polarizability contributions.

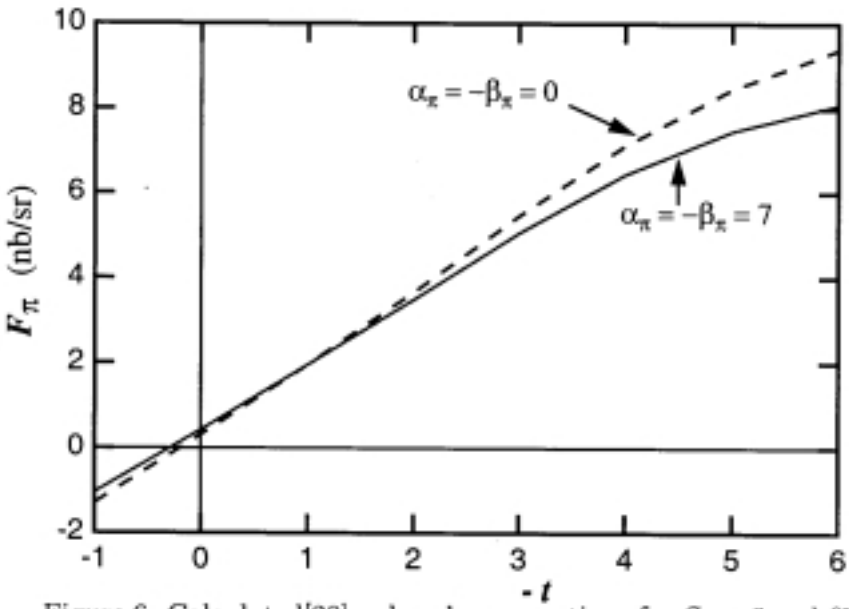

Figure 6: Calculated[28] reduced cross sections for $S_1 = 6$ and $\theta_{\gamma\gamma}^{\rm cm} = 180\,\mathrm{deg}$. The dashed line is the Born result.

5 CLAS Experiment

This measurement of $\vec{\gamma}p \rightarrow \gamma\pi^+n$ requires a 6 GeV electron beam, a tagged polarized photon source, a liquid hydrogen target, and CLAS.

5.1 Photon Source

Even after the data are binned in various kinematic parameters such as S_1, good statistical precision is mandatory for a reliable extraction of the pion polarizability from this experiment. Furthermore, since we seek to measure by time-of-flight a relatively slow neutron in the final state, the experiment has acute sensitivity to background. These two requirements demand a photon source that has very high tagging efficiency and is quite background-free. We therefore believe that the Compton polarized photon source proposed[35] for Hall B is the *only* acceptable source for this particular experiment. With this source, polarized photons with energies up to 1.08 GeV will be produced by the Compton backscattering of 2.4 eV laser light from the 6 GeV Jefferson Lab electrons. The intensity of the electron beam is limited by the beam dump capacity so a high photon flux demands an intense light source. This will be achieved by storing the output of a 10 W laser in a Fabry-Perot resonant cavity with a gain of 30,000 and then colliding the electron beam with the stored light. A flux of about 0.05×10^6 $\vec{\gamma}$-rays/s/MeV is expected for photon energies of about 1000 MeV.

This source has features which make it ideal for the proposed measurements. First, the two-body kinematics of the Compton process strictly limit the energy of photons produced by the backscattering of $E_{laser} = 2.4$ eV photons from electrons with an energy of $E_e = 6.0$ GeV to be less than 1.08 GeV. Unlike the case with bremsstrahlung beams, there will be no flux of untagged high energy photons. Moreover, the two-body character of the kinematics of the reaction being investigated also dictates that there be a fixed relationship between the energy and emission angle of the polarized photon . A suitably sized collimator will limit the energies of the photons on target to be above 500 MeV. In principle then, the Compton source provides 100% tagging efficiency. There will be no background of either low- or high-energy photons

upon the target: neglecting the small inefficiency of the tagging scintillators, every photon that hits the target will be tagged and will lie in the desired energy range. These features cannot be matched by any other photon source.

Second, the cross section for the production of photons varies by no more than a factor of two across the entire photon energy k range, peaking at the highest γ energy and falling as k decreases, while the polarization varies smoothly from almost 100% at the maximum γ energy of 1080 MeV, to about 85% at 600 MeV. As a result, the figure of merit of the $\vec{\gamma}$ beam has its maximum at the highest energies, just where the cross section for photonuclear reaction is the smallest. Moreover, the entire energy range of interest can be covered in a single run.

Third, both the $\vec{\gamma}$ and the "recoiling" electron emerge within very small cones centered on the electron beam direction. The restricted divergence of the γ beam means that the transverse size of the beam on target will only be a few mm. Hence a narrow target can be used with the result that photoproduced charged particles need only pass through a relatively small amount of material in order to reach the CLAS. Furthermore, the divergence of the recoiling electron "beam" will be sufficiently small that the focussing properties of the tagging spectrometer will play no role in determining the energy resolution of the beam. Thus the photon energy will be sufficiently tagged simply by detecting the position of the recoiling electron at a distance from the tagger dipole magnet. Because the required photon energies lie between 0.5 and 1.0 GeV, we will have to detect electrons with energies between 5.0 and 5.5 GeV, *i.e.*, between about 83% and 91% of E_e. This will require a new, albeit simple, detector for the tagging spectrometer. An array of scintillating fibers with a position sensitivity of 1 mm will be adequate to ensure a photon energy resolution of about 1 MeV.

Fourth, there will be no material target in the electron beam. Elevated backgrounds have been experienced in Hall B with the use of the tagged bremsstrahlung photon source. These backgrounds derive from the presence in the beam of a radiating foil. With the proposed Compton source, *there is no radiator*. Instead, the potential sources of background are (electron) beam-gas bremsstrahlung scattering and pair production from the beam collimator. The former should be completely negligible. To first order, the

beam-gas bremsstrahlung flux scales with the product of electron current and gas pressure in the beam pipe. Based on nominal beam currents and vacuum pressures the luminosity for this process at LEGS is 1-2 orders of magnitude higher than in Hall B. Beam neutralization effects make the ratio even more favorable. The $\vec{\gamma}$ flux in Hall B will be at least one order of magnitude higher than at LEGS, so the background to $\vec{\gamma}$ flux ratio in Hall B is 2-3 orders of magnitude lower than at LEGS where it is already almost negligible. The collimator background, also small to begin with, can be significantly reduced by following the collimator with a sweep magnet in order to deflect charged particles photoproduced at the collimator entrance. A second, larger aperture, collimator stops these products. Consequently, backgrounds are expected to be extremely low.

5.2 Target and Detector

The liquid ^{1}H target designed by the Saclay group [36] will be used. The present target cell is 17 cm long, 4.3 cm in diameter, and is constructed of 170 μm mylar foil. Because of the very small size of the $\vec{\gamma}$ beam, the diameter will be reduced to between 1 cm and 2 cm. We believe a 1 cm diameter target could be used. By virtue of its large angular and momentum acceptances, charged particle tracking and momentum reconstruction, and particle identification capabilities, CLAS is an excellent detector for this experiment. Coincident observations of a scattered electron in the tagging spectrometer and π^+ in the CLAS start counter will serve as the trigger for this experiment. The start counter[37] consists of three pieces of plastic scintillator, each 3 mm thick, that surround around the target.

5.3 Particle Detection

The minimum requirements for event reconstruction are a tagged photon, a positively-charged pion, and a recoil neutron in the TOF counter. Although this information is adequate to reconstruct the entire reaction kinematics, the 300 to 600 MeV photons scattered at relatively forward angles may also

be detected in the forward-angle electromagnetic shower counter, albeit with mediocre resolution. This provides valuable independent checks on the kinematic reconstructions and background rejection.

For the selected kinematics, the momentum of the pion ranges from 250 to 600 MeV/c. A magnetic field of one-third to one-half the nominal torus field value provides good acceptance and momentum reconstruction for such pions. Pions will be detected in the start counter and tracked through the drift chambers to the TOF counter, where they can be identified from other charged particles by TOF. In principle, neutrons can be detected in either the TOF counter or electromagnetic calorimeters. However, for this experiment, the 10 to 60 MeV kinetic energy of the neutrons is inadequate to exceed the calorimeter threshold. The TOF counter consists of long scintillator bars situated about 5 meter from the target. These bars are 20 cm wide and 5 cm thick, and light is collected by photomultiplier tubes at each end. From the time difference of the two signals, the azimuthal angle will be given to better than 1° resolution. Similarly, the polar angle is established to about 1° by the position of the hit scintillator bar. As indicated in Fig. 7, the TOF scintillators have about 10% detection efficiency for neutrons in this energy range. This detection efficiency can be precisely calibrated by analyzing $\gamma d \rightarrow pn$ or $\gamma p \rightarrow \pi^+ n$ data. The neutron energy resolution relies on the timing resolution of the TOF counter, $\sigma \approx 150$ ps. With such precision, 1% energy resolution can be expected for neutrons of 10 to 60 MeV, corresponding to a resolution 1 % in t. Finally, the FWHM resolution of the tagged photon beam is assumed to be 2 MeV.

5.4 Event Generator

An event generator was written in order to assess the kinematic distributions of the final-state particles, and to estimate acceptances and resolutions. Starting with a given photon energy, values of S_1 and t are randomly generated ensuring that the event lies within the allowed Chew-Low phase-space shown in Fig. 2. With the fixed values of the three variables k, S_1, and t, the kinematic variables of the recoil neutron can be derived. The kinetic energy

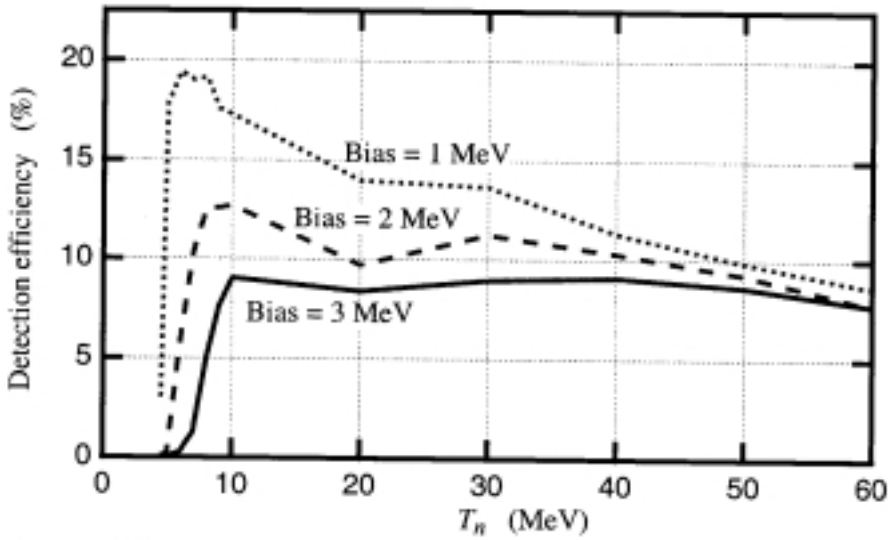

Figure 7: Neutron detection efficiency for 5 cm thick time-of-flight scintillators, calculated using the Kent State code [38].

of the neutron T_n follows from Eq. 2:

$$T_n = \frac{(M_n - M_p)^2 - t}{2M_p} . \tag{15}$$

With p_n and E_n representing the momentum and total energy of the neutron,

$$\begin{aligned} S_1 &= (k + M_p - E_n)^2 - (\vec{k} - \vec{p_n})^2 \\ &= (k + M_p - E_n)^2 - (k^2 - 2kp_n \cos\theta_n + p_n^2) , \end{aligned} \tag{16}$$

and the polar angle of the neutron is given by

$$\cos\theta_n = \frac{S_1 - (k + M_p - E_n)^2 + k^2 + p_n^2}{2kp_n} . \tag{17}$$

The momentum of the virtual pion is equal and opposite to that of the neutron, and it has energy:

$$E_{\pi^0} = M_p - E_n . \tag{18}$$

In the center-of-mass frame, the momentum, energy, and velocity of the $\gamma\pi$ system are

$$\begin{aligned} p_{\gamma\pi} &= (k^2 + p_n^2 - 2p_n k \cos\theta_n)^{\frac{1}{2}} , \\ E_{\gamma\pi} &= k + M_p - E_n , \\ \beta_{\gamma\pi} &= \frac{p_{\gamma\pi}}{E_{\gamma\pi}} \\ &= \frac{(k^2 + p_n^2 - 2p_n k \cos\theta_n)^{\frac{1}{2}}}{k + M_p - E_n} . \end{aligned} \tag{19}$$

In order to determine the event acceptances, random polar and azimuthal angles are generated for the scattered photon relative to the incident photon direction. Within the $\gamma\pi$ system the produced real pion has a momentum opposite to that of the scattered photon. The laboratory system is recovered by means of coordinate rotations and Lorentz boosts.

5.5 Kinematic Resolutions and Acceptances

Event kinematics were generated for photon energy $k = 700$ MeV, $0.5 < -t < 6$, $4 < S_1 < 10$, and $0° < \theta_{\gamma\gamma}^{\rm cm} < 180°$. The response of CLAS for

these events was then simulated using the SDA code[39]. Figure 8 shows the calculated missing mass spectrum. By virtue of the excellent resolution for the pion and recoil neutron, the FWHM missing mass resolution is less than 0.002 GeV^2, much smaller than 0.018 GeV^2, the square of the pion mass. This favors the rejection of potential backgrounds from two-pion production. Figure 9 indicates the corresponding resolution for S_1, less than 1 μ^2. Good resolution in S_1 is important for evaluating the Born term contribution to the Compton cross section. Figures 10-12 show the calculated acceptances as functions of t, S_1, and the center-of-mass scattering angle $\theta_{\gamma\gamma}^{cm}$. All these plots include an assumed neutron detection efficiency of 10%. The lower limit of the neutron kinetic energy was set around 10 MeV, corresponding to a flight time of 120 ns. Because the available range of the TDC extends to 150 ns and the discriminator threshold is $\approx$ 1.5 MeV, $<$ 10 MeV neutrons can be measured in practice, corresponding to events with $-t < 1$.

Of particular importance for event reconstruction is the precise measurement of the π^+ that CLAS provides. However, for backward photon scattering, $\theta_{\gamma\gamma}^{cm} \approx 180°$, pions recoil at small angles relative to the beam direction and are not detected in CLAS. Hence, as seen in Fig. 12, the acceptance for large $\theta_{\gamma\gamma}^{cm}$ is poor. Conversely, for forward-scattered photons the recoil pions are efficiently detected and the acceptance is high. For the kinematic range of interest the recoil neutrons have relatively low kinetic energies, favoring precise momentum measurements by time-of-flight. The photon angular distribution is found to span a large range. Most easily measured in the calorimeter will be the highest energy photons that result from forward scattering.

5.6 Rates

The data event rates rely on the cross section $d^2\sigma \ / \ dtdS_1d\Omega$, however for this experiment the full dependence of this cross section is unknown. The only existing data, from Lebedev[34], are confined to the region $\theta_{\gamma\gamma}^{cm} > 100°$ and are of poor quality. Fil'kov[18, 17] has performed theoretical calculations of the cross section that include diagrams other than the t-channel, one-pion exchange terms. For the kinematics of the Lebedev experiment the results of these calculations are in approximate quantitative agreement with

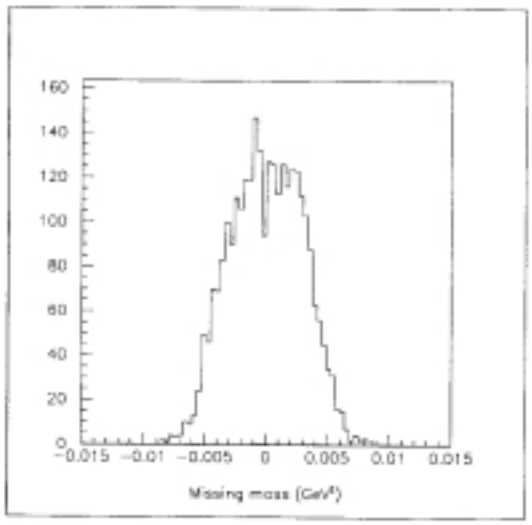

Figure 8: Missing mass spectrum for the reconstruction of the scattered photons. The results are for 700 MeV incident photons, $-t = 2.5$, $S_1 = 6.0$, and $\theta_{\gamma\gamma}^{\rm cm} = 20^o$.

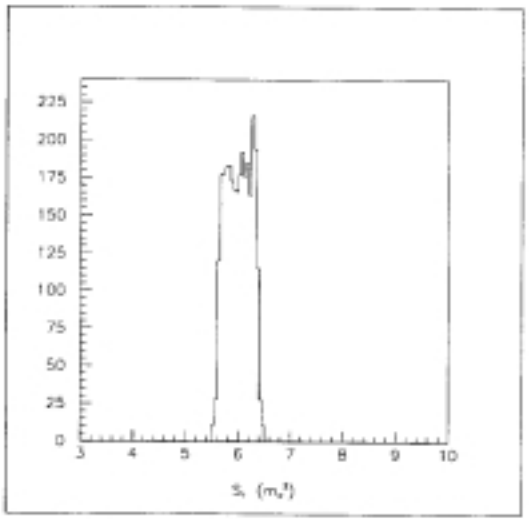

Figure 9: S_1 resolution for $k = 700$ MeV, $-t = 2.5$, $S_1 = 6.0$, and $\theta_{\gamma\gamma}^{\rm cm} = 20°$.

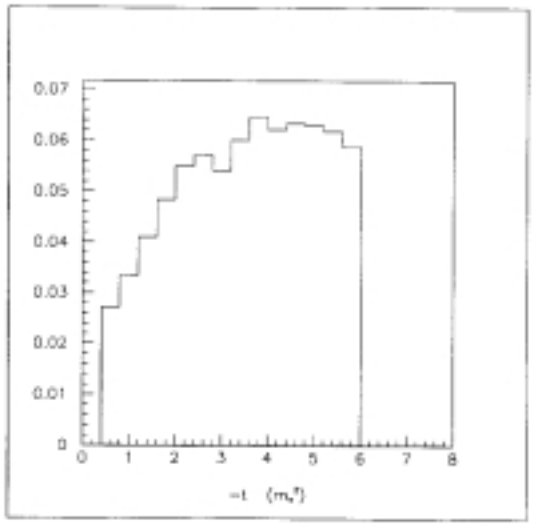

Figure 10: t acceptance for 700 MeV incident photons.

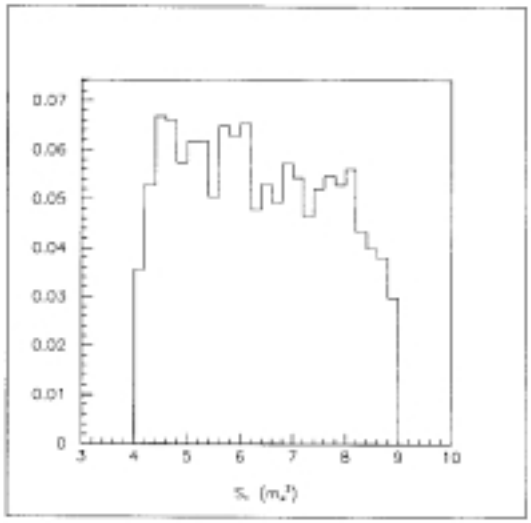

Figure 11: S_1 acceptance for 700 MeV incident photons.

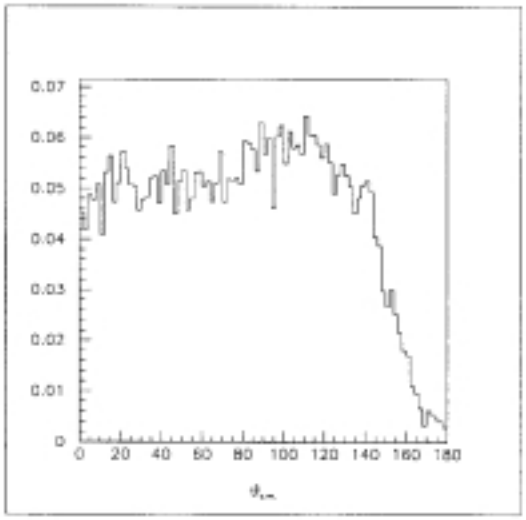

Figure 12: Dependence of the acceptance on the center-of-mass photon scattering angle for 700 MeV incident photons, $-t = 0.5 - 6$ and $S_1 = 4 - 9$.

the data. Nevertheless, Fil'kov's calculations to date are also confined to relatively backward photon scattering angles. Hence, although we have a good indication of the cross section expected for $\theta^{cm}_{\gamma\gamma} > 100°$, there is less information on the size of the cross section at forward angles. For the purposes of estimating event rates in the absence of such information, we assume that the $\gamma p \rightarrow \gamma' \pi^+ n$ cross section *is angle-independent*. Possibly, it could not be all the same. In particular, additional diagrams may have more contribution at forward angles and this would lead certain change on the cross section. However, since we are looking at at low $|t|$ events in a small region of the phase space, this change should not be too large to get a reasonable estimation. On the other hand, the results of Fil'kov that we utilize are for an unpolarized photon beam, but for photons polarized perpendicular to the reaction plane, the contribution of background diagrams is predicted to decrease[17].

To estimate precision, we assume an incident flux of 0.05×10^6 /MeV/s photons in the energy range 700 to 900 MeV. A 20 cm long, liquid hydrogen target is assumed. Table 2 gives the calculated acceptances for a 700 MeV photon beam with coincident detection of the π^+ and neutron. For one full month of beam, a 40° range in the photon scattering angle $\theta^{cm}_{\gamma\gamma}$, and a torus field that is one-half the nominal value, we obtain the event numbers listed in Table 3, the last column of which is the estimated statistical error for the cross section in the corresponding t region. The total number of events for a 30 day run is about 60k, 28 times the number obtained at Lebedev. It should be noted, the above estimation covers only 200 MeV range, including data from 600 to 700 MeV and data from 900 to 1000 MeV, the anticipated precision will be higher.

For an averaged total photoproduction cross section of 220μb and an energy range of 400 MeV, the total trigger rate is about 3.7 kHz. However, due to gaps in the θ and ϕ acceptances of CLAS, the actual trigger rate should be about 1.8 kHz, suitable to the current data acquisition system. This trigger rate can be reduced by an additional 30% by imposing a veto that excludes two-photon events in the calorimeter, events attributed to the π^0 photoproduction. Moreover, for the Compton photon source there is no huge flux of low-energy photons, dramatically decreasing the electromagnetic background in the start counter. The resultant more efficient use of the data acquisition system that will permit us to utilize higher tagged photon fluxes

or cover a wider range in photon energy. In Table 3, the last column lists the estimated statistical error for the cross section in the corresponding t region.

$-t\backslash S_1$	4.5	5.5	6.5	7.5	8.5
0.75	0.068	0.062	0.046	0.036	0.033
1.25	0.062	0.059	0.056	0.043	0.031
1.75	0.060	0.061	0.048	0.043	0.033
2.25	0.070	0.060	0.056	0.047	0.042
2.75	0.063	0.064	0.057	0.046	0.043
3.25	0.065	0.058	0.056	0.054	0.049
3.75	0.069	0.070	0.066	0.060	0.054
4.25	0.065	0.069	0.066	0.059	0.058
4.75	0.068	0.066	0.063	0.057	0.058
5.25	0.049	0.070	0.064	0.061	0.057
5.75	0.041	0.070	0.071	0.066	0.056

Table 2: Acceptance for coincident detection of the pi^+ and recoil neutron for 800 MeV incident photons. A 10 % detection efficiency is included for neutrons.

$-t\backslash S_1$	4.5	5.5	6.5	7.5	8.5	sum	ϵ_σ (%)
0.75	212.	248.	225.	208.	220.	1115.	2.995
1.25	259.	317.	368.	334.	278.	1556.	2.535
1.75	313.	409.	393.	416.	369.	1900.	2.294
2.25	447.	493.	562.	557.	575.	2633.	1.949
2.75	491.	642.	698.	666.	719.	3216.	1.763
3.25	620.	712.	840.	957.	1002.	4132.	1.556
3.75	809.	1056.	1217.	1307.	1357.	5746.	1.319
4.25	941.	1284.	1502.	1586.	1800.	7113.	1.186
4.75	1220.	1523.	1777.	1900.	2231.	8651.	1.075
5.25	1095.	2010.	2247.	2531.	2728.	10611.	0.971
5.75	1144.	2512.	3113.	3420.	3349.	13538.	0.859

Table 3: Overall event numbers for incident $700-900$ MeV photons and one month of beam time.

5.7 Backgrounds

For this experiment the two main sources of background will be from the $\gamma p \to \pi^+ n$ and $\gamma p \to \pi^\circ \pi^+ n$ reactions. Events from the one-pion production reaction can be rejected by applying a cut in missing energy. This reaction has only two particles in the final state and these will be confined to a narrow band in a plot of E_{π^+} versus θ_{π^+}, whereas events from the $\gamma p \to \pi^+ n \gamma$ reaction of interest, will be spread out over a larger phase space. Due to the $\approx 1\%$ energy resolution for measuring the π^+ and the neutron, events having a missing energy of less than 10 MeV, corresponding approximately to the threshold of the calorimeter, should, in principle, be readily distinguishable from two-pion production events provided these are not overwhelmingly abundant. Measurements at Mainz[40] of the total cross section for $\gamma p \to \pi^\circ \pi^+ n$ show it to be 46.5 μb at 779 MeV, roughly 500 times larger than the 0.09 μb cross section predicted for $\gamma p \to \gamma \pi^+ n$. However, at Mainz the total cross section was measured, whereas the $\gamma p \to \gamma \pi^+ n$ cross section is a partial cross section, with kinematic cuts in t, S_1 and photon scattering angle $\theta^{\rm cm}_{\gamma\gamma}$. Thus recourse must be made to theory in order to fairly compare the two cross sections.

For photon energies near 700 MeV the model of Gomez *et al.*[42] underestimates the observed total $\gamma p \to \pi^\circ \pi^+ n$ cross section by about a factor of two. In contrast, calculations by Ochi *et al.*[41], shown in Fig. 13, are in better agreement with experiment and these are therefore preferred for our purposes. The results of Ochi indicate that the restriction of t and S_1, as well as the π^+ and neutron angles to 30°-80° and 20°-50°, respectively as is appropriate for the three-body kinematic distribution, leads to a partial cross section roughly two orders of magnitude smaller than the total $\gamma p \to \pi^\circ \pi^+ n$ cross section for photon energies above 700 MeV. Thus we anticipate that, with the same kinematic cuts, the background $\gamma p \to \pi^\circ \pi^+ n$ cross section should be only several times larger than the $\gamma p \to \gamma \pi^+ n$ reaction of interest. As indicated by Fig. 14, at this level the two reactions can be cleanly separated. Of course, a further reduction of backgrounds can be achieved when scattered photons are detected in the electromagnetic shower counters, as will occur for much of the phase space.

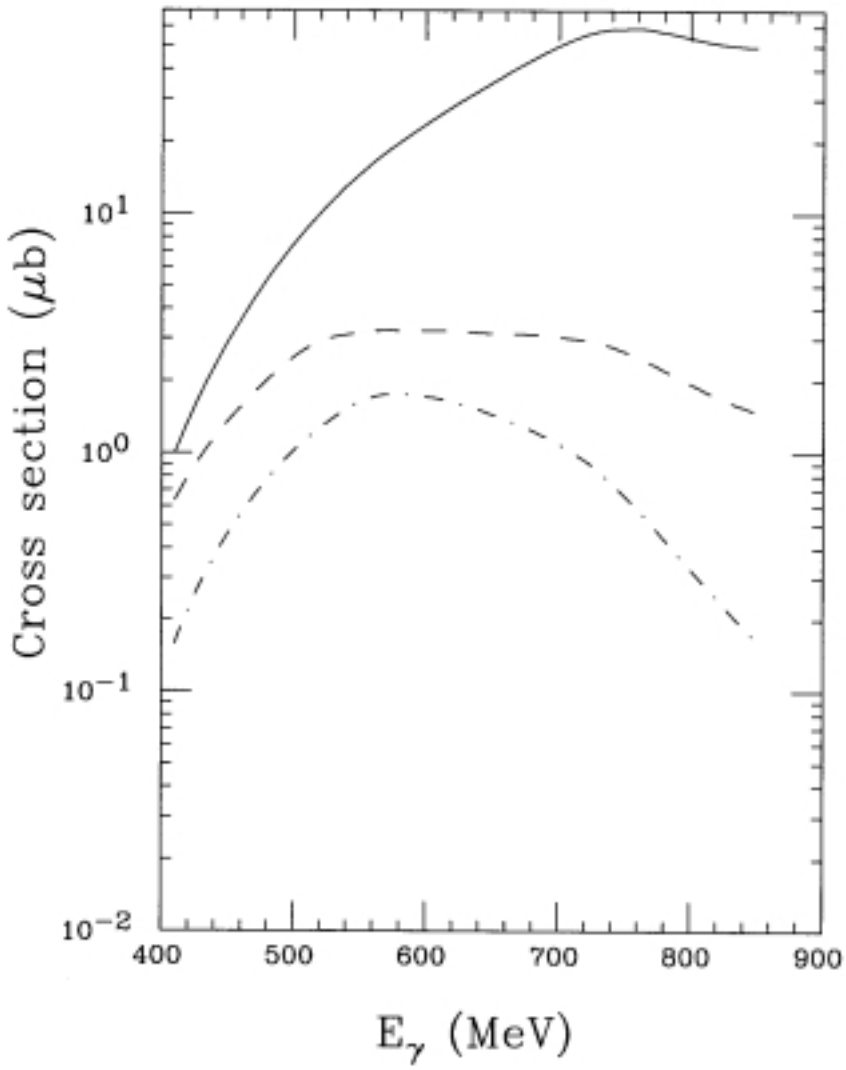

Figure 13: Cross section for two-pion production, calculated by Ochi[41]. The solid curve is the total cross section; dashed curve is for $|t| < 6$ and $9 > S_1 > 4$; and dash-dotted curve includes the additional constraints the angles of the π^+ and neutron are restricted to $30° - 80°$ and $20° - 50°$, respectively.

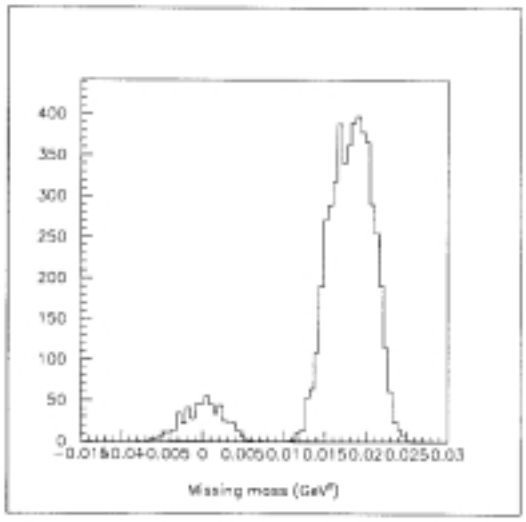

Figure 14: Missing mass spectrum for the $\gamma p \rightarrow \pi^{o}\pi^{+}n$ reaction with an unobserved π^{o}. The calculations are for 700 MeV photons, $-t = 2.5$, $S_1 = 6.0$, and $\theta_{\gamma\gamma}^{cm} = 20^{o}$. The number of π^{o} production events was assumed to be ten times than photon scattering events.

5.8 Projected Results

Estimated uncertainties for the polarizability difference $\bar{\alpha} - \bar{\beta}$ and sum $\bar{\alpha} + \bar{\beta}$ are shown in Table 4. The results, for a one-month run with the numbers of events given in Table 3, include the extrapolation error as well the resolution uncertainty in S_1, the invariant squared mass of the γ-π system. Following the extrapolation to the pion pole, the dominant Born contribution must be subtracted. This is exactly calculable, provided S_1 and $\theta^{\rm cm}_{\gamma\gamma}$ are known. In the present case, however, the experimental resolution for S_1 and $\theta^{\rm cm}_{\gamma\gamma}$ is good enough such that their effect on the overall error is insignificant compared to the extrapolation uncertainty. The overall projected uncertainty of $< 1 \times 10^{-4}$ fm^3 in $\bar{\alpha} + \bar{\beta}$ is about one order-of-magnitude better than the overall uncertainty in $\bar{\alpha} - \bar{\beta}$. As previously noted, one reason for this is that the polarizability difference is most important at backward photon scattering angles for which the pion, recoiling in the forward direction, may avoid detection. In addition, compared to the polarizability difference, in the expression for the Compton cross sections the polarizability sum is favored by a factor of S_1.

The results given in Table 4 assume, in accord with present theoretical predictions, that $F(t)$ has a near-linear dependence within the t-range of the data and extrapolation. In particular, there is no consideration of the model-dependence of $F(t)$. An indication of the effect of this model-dependence is that a curvature in $F(t)$ amounting to a 10% quadratic contribution over the range of the data and extrapolation would change the linearly-extrapolated value of $\bar{\alpha}+\bar{\beta}$ by $\approx 1\times10^{-4}$ fm^3. Thus we attribute to model- dependence an uncertainty comparable to the overall error due to extrapolation of data that have statistical limits. For larger S_1 the Born term decreases with the result that the expected precision for both $\bar{\alpha}-\bar{\beta}$ and $\bar{\alpha}+\bar{\beta}$ improves. Of course, the values obtained for the polarizabilities should not depend on S_1. However, in order to test the reliability of the extrapolation procedure, it is valuable to obtain independent results for different ranges of S_1. The table shows that meaningful comparisons could be made between different S_1 ranges for $\bar{\alpha}+\bar{\beta}$, but not for $\bar{\alpha} - \bar{\beta}$. The overall uncertainty projected for $\bar{\alpha} - \bar{\beta}$ is comparable to the expected magnitude of the term itself. By itself, this would not merit a CLAS experiment to determine the polarizability difference. In contrast, the

S_1	$5-6$	$6-7$	$7-8$	$8-9$	$9-10$	$5-10$
$\bar{\alpha}-\bar{\beta}$	36.8	24.0	16.8	12.5	10.4	6.7
$\bar{\alpha}+\bar{\beta}$	6.7	3.7	2.2	1.5	1.1	0.8

Table 4: Projected uncertainties of values extracted for the polarizability difference and polarizability sum. Results are given for various bins in the invariant squared mass of the $\gamma\pi$ system.

uncertainty projected for the polarizability sum $\bar{\alpha}+\bar{\beta}$ represents a significant improvement over the previous experimental determination, enabling us to better test the theoretical notion that $\bar{\alpha}+\bar{\beta}\approx 0$.

The comprehensive acceptance of CLAS facilitates additional checks on the reliability of the analysis. For example, the extracted polarizability contribution should also be independent of the Treiman-Yang angle, the angle between the scattering and production planes. Furthermore, with CLAS measurements will be automatically made over the full range of ϕ, the angle between the plane of polarization of the incident photon beam, and the scattering plane. The polarizability contribution to the cross section has a known dependence on ϕ, and this can be checked. Data will also be obtained in medium $\theta_{\gamma\gamma}^{cm}$ kinematic regions, where the polarizability contribution to the Compton cross section is known to be negligible. With these data, we can extrapolate to a Compton cross section that is defined by the precisely-calculable Thomson limit. Finally, possible singularities in the extrapolation path to the pion pole[17] must be avoided. The large acceptance of CLAS makes it straightforward to do this. The power of the combination of CLAS and the backscattering Compton polarized photon source is that all these various measurements are made simultaneously, no separate beam or detector set-ups are required. We consider this capability to be one of the most compelling justifications for using CLAS to investigate the Compton scattering from the pion.

5.9 Comparison with Other Experiments

As previously noted, a new series of experiments have been proposed to study Compton scattering from pions. For example, the $\gamma\gamma \to \pi\pi$ reaction constitutes part of the core research program of the DaΦne collider, recently commissioned in Frascati. The second DaΦne handbook[43] contains detailed consideration about what the $\gamma\gamma \to \pi\pi$ reaction can say regarding pion polarizabilities. As previously indicated, this subject has generated considerable controversy. Nevertheless, the conclusion is expressed, *within the* DaΦne *handbook*, that whereas there are good reasons for measuring $\gamma\gamma \to \pi\pi$ reaction, *it is not a means by which one should attempt to determine the pion polarizability.*

A separate experimental effort[28] is approved at Mainz to measure the pion polarizability using radiative photoproduction, the same reaction we seek to exploit at JLab. This experiment has an advantage over the proposed JLab investigation in that the the Mainz investigation will employ an array of BaF_2 crystals capable of measuring the scattered photons with an energy resolution of $3 - 5\%$, about four times better than CLAS can achieve. At Mainz, produced pions will be detected using a forward planes of multi-wire proportional chambers, and, as with the JLab proposal, neutrons are to be measured by TOF scintillators. While this detector configuration provides versatility lacking in CLAS, it does not have the comprehensive acceptance CLAS offers. In particular, because their detectors are restricted in their solid angle coverage, the Mainz experiment is configured to measure exclusively the backward-angle photon scattering that is sensitive to the polarizability difference. It is projected that $\bar{\alpha} - \bar{\beta}$ will be determined with an extrapolation uncertainty of approximately 3×10^{-4} fm^3. A determination of the sum $\bar{\alpha} + \bar{\beta}$ would require a different detector set-up, and this has not been proposed.

Additional differences distinguish the JLab and Mainz experiments. At Mainz it is intended to utilize photons from the high-rate GEM tagging facility[44] that is presently under development. While this facility has the potential to tag photons at rates up to 3×10^8 Hz, it utilizes a bremsstrahlung radiator, and hence a large flux of untagged photons will be directed on the target. Consequently, backgrounds will be more difficult to deal with than at

CLAS. Moreover, the photon beam tagged by GEM will be unpolarized, and hence, as with the more restricted detector acceptance, there is no capability of using this tool as a means for ensuring the reliability of the extrapolation to the pion pole. To summarize, we consider the Mainz and JLab studies to be complementary. The versatility of the relatively simple Mainz set-up permits a determination of the polarizability difference. The JLab experiment would be sensitive to the polarizability sum, and provide the extensive detector acceptance that is critical for testing the systematics of the extrapolation needed to determine Compton scattering from the pion.

The COMPASS[45] collaboration at CERN also includes a determination of the polarizability of the pion among its broad range of goals. To be commissioned in 1999, COMPASS will employ a fixed targets and beams of muons, pion, kaons, and protons with momenta up to 300 GeV/c. Particles will be detected by the forward magnetic spectrometers that include drift-chamber tracking and lead-glass calorimetry. RICH counters provide particle identification, and the electronics feature dedicated triggers and fast read-out. The polarizability of the pion will be determined[46] from the Primakoff process of pion scattering from virtual photons in the field of a heavy nucleus. Kaon polarizabilities will likewise be investigated using kaon beams. In the meson rest frame, the equivalent energy of incident photons ranges from 100-2000 MeV. These studies rely upon the identification of the Primakoff cross section by means of its strong peaking at very small t. Similar to the cross section measured in radiative photoproduction, the Primakoff cross section is mainly given by the Thomson term, but also contains contributions from the electric and magnetic polarizabilities that vary according to the photon scattering angle $\theta_{\gamma\gamma}^{cm}$ in the meson rest frame. Values for both $\bar{\alpha}$ and $\bar{\beta}$ may be extracted by fitting data over the full range of $\theta_{\gamma\gamma}$ angles that COMPASS has access to. It is projected[46] that for a COMPASS pion beam rate of 5 MHz about 2×10^6 Primakoff events per month should be observed, yielding polarizabilities with statistical uncertainties of the order of 0.2, considerably better than will be achieved in the proposed JLab experiment.

Perhaps the main concern regarding the COMPASS experiment are backgrounds, for example the high rate of non-interacting beam pions that enter the forward spectrometer. The Primakoff trigger is designed to reject this background. Although several other backgrounds[47], both strong and elec-

tromagnetic, are also present, these do not display the low-t peaking that is the signature of the Primakoff process. As a result, most backgrounds can be assessed by extrapolating to low-t their contributions observed at higher t. What is important then is the relative size of the Primakoff and background contributions at low-t, but this remains to be established.

Another attempt[46] to determine the pion polarizabilities by means of radiative pion scattering was recently made in the SELEX/E781 experiment at Fermilab using a mixed pion-hyperon beam of 600 GeV. This experiment yielded only limited statistics for Primakoff events. Moreover, the SELEX beam was of a size that made it difficult to distinguish Primakoff pions from non-interacting beam pions. Although the COMPASS experiment has much promise, the issue of backgrounds remains to be confronted. Recall also that the single published radiative pion scattering measurement[19] gave $(6.8 \pm 1.4 \pm 1.2) \times 10^{-4}$ fm^3 for the electric polarizability, a value that disagrees with the 2.7×10^{-4} fm^3 that is the firm prediction of chiral symmetry. The different experimental approaches have given results for the pion polarizability that disagree.

In the absence of a free pion or photon target, there is no experimentally clean means of determining pion polarizability. All experimental methods are subject to appreciable backgrounds, and, polarizability generally provides only a small correction to the Compton cross section. Consistency between the results of various experiments is essential for a satisfactory experimental understanding of pion polarizability. Experimentally, radiative pion photoproduction and radiative pion scattering are subject to different types of backgrounds, and the analysis procedures also differ. Hence consistency between these two methods would serve to establish experimental values for pion polarizability that are on a much more secure footing.

6 Summary

We seek one month of beam time in order to investigate the polarizabilities of the charged pion. Our method relies upon pion photoproduction using a back-scattering Compton source to provide polarized photons between 600 and 1000 MeV. The Compton photon source in particular is characterized by high flux, high polarization, and low background. The combination of the polarized photon source and the CLAS detector is particularly well-suited for a determination of the sum of the electric and magnetic pion polarizabilities, $\bar{\alpha} + \bar{\beta}$. Indeed, Chiral Perturbation Theory makes a firm prediction, for up to four pion loops, that $\bar{\alpha} + \bar{\beta} = 0$. A six-loop calculation yields $\bar{\alpha} + \bar{\beta} = 0.3 \times 10^{-4}\text{fm}^3$. A one-month run using CLAS will permit us to test this prediction to a precision of better than $1 \times 10^{-4}\text{fm}^3$, an improvement of almost one-order of magnitude over the only previous experimental determination of the polarizability sum, derived from radiative pion scattering. This would permit us to make a needed check of the convergence properties of ChPT.

The polarizabilities of the pion have heretofore resisted precise determination. Experiments are in the planning stages at a number of laboratories, but none of these experiments will be easy. Nevertheless, by means of a multi-pronged attack that draws upon the diverse strengths of different facilities, we can expect that the experimental situation regarding the pion polarizabilities will be significantly improved during the next few years. At CLAS we have a real opportunity to contribute to this progress.

References

[1] V. Bernard and W. Weise, Phys. Lett. **B159**, 85 (1988).

[2] V. Bernard and D. Vautherin, Phys. Rev. **D40**, 1615 (1989).

[3] V. Petrun'kin, Sov. J. Part. Nucl. **12**, 278 (1981).

[4] L. Fil'kov *et al.*, Phys. Rev. **D26**, 3146 (1982).

[5] D. Babusci *et al.*, Phys. Lett. **B277**, 158 (1992).

[6] B. Holstein, Comm. Nucl. Part. Phys. **19**, 221 (1990).

[7] B. Holstein, Nucl. Phys. **A546**, 213 (1992).

[8] A. L'kov and V. Petrun'kin, JETP Lett **37**, 63 (1983).

[9] J. Gasser and H. Leutwyler, Nucl. Phys. **B250**, 465 (1985).

[10] J. Donoghue and B. Holstein, Phys. Rev. **D40**, 2378 (1989).

[11] V. Bernard and W. Weise, Phys. Lett. **238**, 111 (1990).

[12] K. Kawarabayashi and M. Suzuki, Phys. Rev. Lett. **16**, 255 (1966).

[13] Riazuddin and Fayyazuddin, Phys. Rev. **147**, 1071 (1966).

[14] M. Ivanov and T. Mizutani, Phys. Rev. **D45**, 1580 (1992).

[15] G. Chew *et al.*, Phys. Rev. **106**, 1345 (1957).

[16] H. Primakoff, Phys. Rev. **31**, 899 (1951).

[17] D. Drechsel and L. Fil'kov, Z. Phys. **A349**, 177 (1994).

[18] T. Aibergenov *et al.*, Czech. J. Phys. B **36**, 948 (1986).

[19] Y. M. Antipov *et al.*, Phys. Lett. **121B**, 445 (1983).

[20] Y. M. Antipov *et al.*, Z. Phys. **C26**, 495 (1985).

[21] C. Berger *et al.*, Z. Phys. **C26**, 199 (1984).

[22] A. Courau *et al.*, Nucl. Phys **B271**, 1 (1986).

[23] Z. Ajaltoni *et al.*, DM2 Coll, VII Int. workshop on photon-photon collision, Paris, 1986.

[24] J. Boger *et al.*, Phys. Rev. **D42**, 1350 (1990).

[25] H. Marsiskie *et al.*, Phys. Rev. **D42**, 1350 (1990).

[26] Kaloshin94, Phys. Atom. Nucl. **57**, 2207 (1994).

[27] J. Portoles and M. Pennington, The Second DaΦne handbook INFN-Laboratori Nazionali di Frascati http://hpteor.lnf.infn.it/dafne.html, 1995.

[28] Ahrens, private communication, Proposal at Mainz, 1996.

[29] Kowalewski *et al.*, Phys. Rev. **D29**, 1000 (1984).

[30] R. Walker *et al.*, High Energy Phys., Proc. Ann. Rochester **10**, 17 (1960).

[31] P. Cziffra *et al.*, Nucl. Phys. **36**, 258 (1962).

[32] G. Smith *et al.*, Phys. Rev. Lett. **5**, 571 (1960).

[33] R. Miskimen, K. Wang, and A. Yegneswaran, CEBAF Proposal, 94-015, 1994.

[34] T. Aibergenov *et al.*, Proc. of the Lebedev Phys. Inst. **186**, 169 (1988).

[35] B. Norum and P. Welch, CEBAF Letter of intent 93-012, 1993.

[36] C. Marchand, private communication, Liquid target, 1995.

[37] G. Mutchler, private communication, Start counter, 1995.

[38] B. Anderson, private communication, Neutron efficiency code from Kent State University, 1997.

[39] B. Niczyporuk, private communication, SDA code, 1995.

[40] A. Braghieri *et al.*, Phys. Lett. **B363**, 46 (1995).

[41] K. Ochi *et al.*, private communication and LANL preprint nucl-th/9703058 and nucl-th/9711031, 1997.

[42] J. G. Tejedor and E. Oset, Nucl. Phys **A600**, 413 (1986).

[43] The Second DaΦne handbook INFN- Laboratori Nazionali di Frascati http://hpteor.lnf.infn.it/dafne.html, 1995.

[44] I. Anthony *et al.*, Nucl. Instrum. and Meth. **A301**, 230 (1991).

[45] Common Muon and Proton Apparatus for Structure and Spectroscopy; CERN/SPSLC 96-14 http://www.compass.cern.ch/compass/proposal/, 1996.

[46] M. A. Moinester and V. Steiner, Proc. of the CERN COMPASS Summer School, Prague, Czech Republic, Aug. 1997 (hep-ex/9801011), 1997.

[47] M. A. Moinester, Pion and Sigma Polarizabilities and Radiative Transitions, in Chiral Dynamics: Theory and Experiment, Ed. A. Bernstein and B. Holstein, Springer-Verlag (hep-ph/9409463), 1994.